High-precision (p,t) reaction to determine ^{25}Al$(p,\gamma)^{26}$Si reaction rates

A. Matic,[*] A. M. van den Berg, M. N. Harakeh,[†] and H. J. Wörtche
Kernfysisch Versneller Instituut, University of Groningen, Zernikelaan 25, NL-9747 AA Groningen, The Netherlands

G. P. A. Berg, M. Couder, J. Görres, P. LeBlanc, S. O'Brien, and M. Wiescher
Department of Physics and the Joint Institute for Nuclear Astrophysics, University of Notre Dame, Notre Dame, Indiana 46556, USA

K. Fujita, K. Hatanaka, Y. Sakemi, Y. Shimizu,[‡] Y. Tameshige,[§] A. Tamii, and M. Yosoi
Research Center for Nuclear Physics, Osaka University, Ibaraki, Osaka 560-0047, Japan

T. Adachi, Y. Fujita, and Y. Shimbara
Department of Physics, Osaka University, Toyonaka, Osaka 560-0043, Japan

H. Fujita
School of Physics, University of the Witwatersrand, P.O. Wits, Johannesburg 2050, South Africa

T. Wakasa
Department of Physics, Kyushu University, Fukuoka 812-8581, Japan

B. A. Brown and H. Schatz
Department of Physics and Astronomy, National Superconducting Cyclotron Laboratory and the Joint Institute for Nuclear Astrophysics, Michigan State University, East Lansing, Michigan 48824, USA
(Received 15 June 2010; published 18 August 2010)

Since the identification of ongoing ^{26}Al production in the universe, the reaction sequence ^{24}Mg$(p,\gamma)^{25}$Al$(\beta^+\nu)^{25}$Mg$(p,\gamma)^{26}$Al has been studied intensively. At temperatures where the radiative capture on ^{25}Al ($t_{1/2} = 7.2$ s) becomes faster than the β^+ decay, the production of ^{26}Al can be reduced due to the depletion of ^{25}Al. To determine the resonances relevant for the ^{25}Al$(p,\gamma)^{26}$Si bypass reaction, we measured the ^{28}Si$(p,t)^{26}$Si reaction with high-energy precision using the Grand Raiden spectrometer at the Research Center for Nuclear Physics, Osaka. Several new energy levels were found above the p threshold and for known states excitation energies were determined with smaller uncertainties. The calculated stellar rates of the bypass reaction agree well with previous results, suggesting that these rates are well established.

DOI: 10.1103/PhysRevC.82.025807 PACS number(s): 25.40.Hs, 26.30.Ca, 26.50.+x, 27.30.+t

I. INTRODUCTION

The origin of long-lived radioactive isotopes in our universe has been one of the most interesting questions in nuclear astrophysics. They serve as unique signatures for nucleosynthesis and nucleosynthesis patterns for explosive events such as novae and supernovae. In particular, the production mechanism and the production site of long-lived ^{26}Al ($t_{1/2} = 0.72$ Ma) have been of prime interest for several decades after the first indications of ^{26}Al enrichment were determined from ^{26}Mg/^{24}Mg abundance ratios in meteoritic inclusions [1,2]. It has been argued that ^{26}Al after its production during the carbon-burning phase of a nearby presupernova star was injected into the presolar material by the subsequent supernovae explosion and decayed *in situ* after condensation causing a local enrichment of ^{26}Mg [3,4]. A number of alternative production sites have been proposed, for example, the shock waves of explosive hydrogen burning in supernovae traversing the outer hydrogen-rich layers of presupernova stars [5], the explosive hydrogen burning in novae [5,6], and the surface of the meteoritic material [7] where ^{26}Al may be produced by cosmic rays. The continuing production of ^{26}Al has been clearly supported by the observation of the 1.809-MeV γ-ray decay line of ^{26}Al with satellite-based γ-ray observatories such as HEAO-C [8] and the COMPTEL detector on the NASA Compton Gamma Ray Observatory (CGRO) [9]. These early observations have spawned additional predictions about ^{26}Al-production sites such as Wolf-Rayet stars [10] or the complex burning environments of asymptotic giant branch (AGB) stars [11,12]. Both observations associated a large production of ^{26}Al with the inner galaxy but the COMPTEL

[*]Present address: Forschungszentrum Dresden-Rossendorf, Postfach 510119, 01314 Dresden, D-01328 Dresden, Germany.
[†]Present address: GSI Helmholtzzentrum für Schwerionenforschung GmbH, Planckstraße 1, D-64291 Darmstadt, Germany.
[‡]Present address: Center for Nuclear Study, University of Tokyo, Wako, Saitama 351-0198, Japan.
[§]Present address: Office for Development of Proton Therapy Center, Regional Health Services Division, Department of Health and Welfare Fukui Prefectural Government, Fukui City, Fukui Prefecture 910-0846, Japan.

results also demonstrated a strong correlation between ^{26}Al enrichment and known sites of supernovae remnants. This clearly reduced the likelihood of substantial ^{26}Al contributions from alternative production sites such as novae or AGB stars [11] and pointed toward core-collapse supernovae or associated nucleosynthesis processes in massive presupernova stars [13] as most likely sources for ^{26}Al. This does not preclude possible contributions from novae [14] or AGB stars [15], but massive stars with late stellar evolution and subsequent core-collapse nucleosynthesis seem to be the primary sites for ^{26}Al production [13].

Simulations of nucleosynthesis demonstrate that there are three distinct processes by which ^{26}Al can be produced in massive stars and supernovae explosions, namely, core and shell hydrogen burning, carbon shell burning, and explosive neon burning [16]. All three processes produce ^{26}Al through the ^{25}Mg$(p,\gamma)^{26}$Al reaction. This requires the presence of both ^{25}Mg and hydrogen fuel. The abundance of ^{25}Mg in hot hydrogen burning environments depends sensitively on the MgAl cycle [17], which also drives the ^{26}Al production in ONeMg novae [14]. The critical reaction sequence leading to the production of the long-lived 5^+ ground-state configuration of ^{26}Al is ^{24}Mg$(p,\gamma)^{25}$Al$(\beta^+\nu)^{25}$Mg$(p,\gamma)^{26}$Al. At temperatures of typically $\geqslant$0.5 GK the proton capture on ^{25}Al ($t_{1/2} = 7.2$ s) is predicted to become faster than the competing β decay, leading to the production of ^{26}Si. These high-temperature conditions are expected for both shell carbon burning and explosive neon burning, which take place at substantially higher temperatures [13]. ^{26}Si decays predominantly to the short-lived first-excited 0^+ isomeric state ($t_{1/2} = 6.3$ s) in ^{26}Al*, which decays primarily to the ground state of stable ^{26}Mg or is depleted by proton capture on ^{26}Al*$(p,\gamma)^{27}$Si [18]. The high-temperature branch or proton capture on ^{25}Al, therefore, might lead to a significantly reduced ground-state production of ^{26}Al under high-temperature conditions and depends sensitively on the reaction rate of ^{25}Al$(p,\gamma)^{26}$Si.

So far, no direct experimental study of ^{25}Al$(p,\gamma)^{26}$Si has been made because it requires the production of intense radioactive ^{25}Al beams. A number of predictions have been made to explore the contributions of various reaction rates on the basis of limited existing experimental data and shell-model predictions with large uncertainties of the level structure of the ^{26}Si compound nucleus [17,19–21]. To reduce the uncertainties in the experimental input parameters, namely, the excitation energies and the spin and parity assignments, several studies have been performed to probe possible resonance contributions to the reaction cross section. These studies were based on a number of different reactions populating the proton-unbound states in ^{26}Si, such as the ^{28}Si$(p,t)^{26}$Si two-neutron pickup [22–24], the ^{29}Si$(^3$He,^{6}He$)^{26}$Si three-neutron pickup [25], and the ^{24}Mg$(^3$He,$n)^{26}$Si two-proton stripping reactions [26]. Complementary to these particle-transfer techniques in-beam γ-ray spectroscopy has been utilized to probe the level scheme with high resolution [27]. While direct-radiative-capture measurements have not yet been performed because of the lack of sufficiently high ^{25}Al beam intensities, first measurements using the single-particle transfer reaction ^{25}Al$(d,n)^{26}$Si have been successfully completed at the RESOLUT radioactive-ion beam facility at Florida State University [28]. The results suffer from low resolution but provide a first glimpse of the actual resonance strength which had been estimated previously from shell-model predictions or mirror-state analysis with large uncertainties.

While most of the previous studies have addressed the critical question of spin assignments for the various resonance states in ^{26}Si, the present study is focused on a high-precision measurement of the excitation energies using the ^{28}Si$(p,t)^{26}$Si reaction. The measurement was performed at the high-resolution Grand Raiden (GR) spectrometer at the Research Center for Nuclear Physics (RCNP) cyclotron facility in Osaka, Japan, which provides substantially better resolution than previously achieved for this reaction with Si detector arrays [22,24] or classical magnetic split pole spectrometers [23]. A reduction in the experimental uncertainties of the excitation energies will translate directly into a reduction of the uncertainties in the calculated reaction rates. In this sense the data presented here complement the recent study of high-resolution in-beam γ-spectroscopy techniques [27] that was limited to γ-decay measurements below and near the proton threshold in ^{26}Si.

In the following section we describe the experiment and the experimental arrangements. In Sec. III we present the experimental results and compare those with the results from previous studies. In Sec. IV we discuss the implications for the calculated reaction rates of ^{25}Al$(p,\gamma)^{26}$Si.

II. EXPERIMENTAL TECHNIQUE AND ENERGY CALIBRATION

We performed a ^{28}Si$(p,t)^{26}$Si experiment at RCNP. The experimental conditions were similar to those of the previously reported ^{24}Mg$(p,t)^{22}$Mg [29] experiment. Here, we briefly summarize the setup and report details relevant for this particular experiment. A proton beam with an energy of (98.7 ± 0.1) MeV from the Ring Cyclotron was transported via the "fully dispersion-matched" WS beam line [30] to a target chamber at the entrance of the Grand Raiden spectrometer [31]. When using an achromatically tuned beam on the target the spectral resolution is limited by the energy spread of the beam, that is, $\approx$100 keV in this experiment. The benefit of lateral dispersion matching is that it allows measurements with resolutions as good as the resolving power of the spectrometer, that is, $p/\Delta p = 37\,000$ corresponding to $\approx$5 keV in this experiment. However, this would have required very thin targets and therefore too long measurements or poor statistics. In this experiment the thickness of the ^{28}Si self-supporting target with an isotopic enrichment of 99.94% was 0.7 mg/cm^2, a compromise between high resolution and sufficient count rates. This resulted in an excellent resolution of about 13 keV. The target consisted of a stack of three thin metallic layers and was produced as described in Ref. [32]. The outgoing tritons were momentum analyzed by using the GR spectrometer.

In addition, we collected also spectra using a 1.86 mg/cm^2 thick natural Si target at all three spectrometer angles. By comparing differential cross sections for the ^{26}Si levels measured at different time intervals on both Si targets (enriched and natural) we concluded that one of the three layers was

TABLE I. Low-lying levels of ^{26}Si with excitation energies in MeV, up to the proton-emission threshold, that were considered in our energy calibration.

Ref. [34] (^{3}He,n)	Ref. [27] ^{16}O(^{12}C,2n)^{26}Si	Arithmetic average	Difference	Calibration error
g.s.	g.s.	g.s.[a]	–	–
1.7959(2)	1.7973(1)	1.7966[a]	0.0007	0.0008[a]
2.7835(4)	2.7864(2)	2.7850[a]	0.0014	0.0017[a]
3.3325(3)	3.3364(6)	3.3345[a]	0.0019	0.0025[a]
3.756(2)	3.7569(2)	3.7565	0.0004	0.0006
3.842(2)	–	–	–	–
4.093(3)	–	–	–	–
4.138(1)	4.1393(7)	4.1387	0.0007	0.0014
–	4.1871(3)	–	–	0.0014
4.445(3)	4.4462(4)	4.4461[a]	0.0001	0.0005[a]
–	4.7985(5)	–	–	0.0016
4.805(2)	4.8107(6)	4.8084	0.0023	0.0029
–	4.8314(10)	–	–	0.0021
–	5.1467(9)[a]	–	–	0.0020[a]
–	5.2882(5)	–	–	0.0016
–	5.5172(5)[a]	–	–	0.0016[a]
–	5.5677(17)	–	–	0.0028

[a]Energies and errors in MeV used in the present calibration. For the calculation of the error used in the calibration, see text.

burned at the beginning of the measurements and a second one later on. Therefore, the statistics is much lower compared to the ^{24}Mg measurement discussed in Ref. [29] that was performed under otherwise identical conditions. For the identification and subtraction of events from the observed ^{12}C and ^{16}O contaminants, a 1 mg/cm^2 thick natural carbon and a 1 mg/cm^2 thick Mylar target were used. A more detailed description of experimental conditions can be found in Refs. [29,33].

The best-possible energy calibration is important for the precision of the stellar-rate calculations. Therefore, careful consideration had to be given to several factors that affect the calibration. These include a small quadratic deviation from the linear momentum (p) versus focal-plane position (x) calibration, the beam energy, and the proper scaling procedures when the magnetic field was changed. A detailed account of these effects is given in Refs. [29,33]. In the following we discuss the calibration procedures that are specific for the measured ^{28}Si(p,t)^{26}Si reaction.

The recently published high-precision ^{26}Si γ-spectroscopic study by Seweryniak *et al.* [27] ruled out levels at 3.842- and 4.093-MeV excitation energies that were reported by Bell *et al.* [34]. Also, several excitation energies measured in both studies do not agree within the rather small errors, as can be seen by comparing the first and second column of Table I. Therefore, we used the arithmetic average of these energies, which is shown in column 3. The calibration error (column 5) is calculated by adding the differences (column 4) between the averages and the original values and the errors of Ref. [27]. For the two levels at 5.1467 and 5.5172 MeV observed only by Seweryniak *et al.* [27], we added an error of 1.1 keV, that is, the average difference of the seven levels observed in both studies. In Table I, level energies and their uncertainties used for the present calibration are marked by an asterisk. In this article we quote results obtained by Bell *et al.* [34] and Seweryniak *et al.* [27] with the modified errors and not the originally quoted ones.

The energy calibration obtained from the ^{28}Si(p,t)^{26}Si data was in excellent agreement with the calibration from the ^{24}Mg(p,t)^{22}Mg spectra [29] except for a small shift that can be attributed to the uncertainty in the mass of ^{26}Si and the beam energy. Changing the beam energy by 100 keV resulted in a change of ^{26}Si excitation energies of up to 1.5 keV for states at high excitation energies. The error of the ^{26}Si excitation energies includes the uncertainty of the x position in the focal plane as statistical error. The systematic error includes errors originating from the uncertainties of the reaction angle, the mass of ^{26}Si (1 keV), and the beam energy. The resulting three systematic errors are quadratically added to obtain the total systematic error. The systematic and statistical errors are linearly added to obtain the total error. This error is used for the present ^{26}Si data.

III. EXPERIMENTAL RESULTS

The goal of this experiment was to investigate the nuclear structure of ^{26}Si from the ground state up to about 9-MeV excitation energy. This covers the energy range well above the proton threshold of 5.5123 MeV where resonance levels of the ^{25}Al(p,γ)^{26}Si reaction are expected within the Gamow window for temperatures up to about 1.5 GK. The well-known natural parity states at lower excitation energies are used for

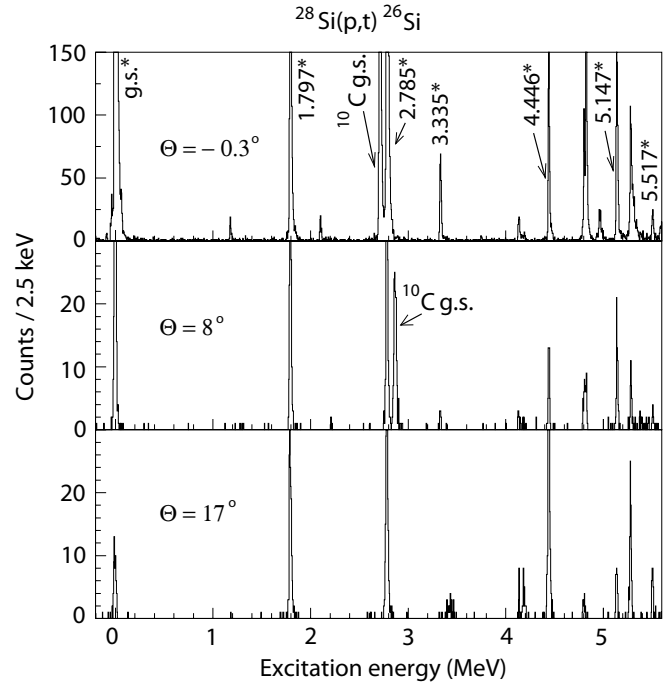

FIG. 1. The ^{28}Si(p,t)^{26}Si spectra of the low-lying energy levels measured at spectrometer angles of −0.3°, 8°, and 17°. The excitation energies of the levels marked with an asterisk in this figure and also in Table I were used in the energy calibration.

calibrating the observed spectra. This and the good resolution allowed very precise determination of the resonance energies. Because of the small momentum acceptance of 5% of GR [31] measurements were necessary at two different magnet settings to cover the full excitation energy range. The measurements were performed at three angle settings of GR, −0.3°, 8°, and 17°, to allow the identification of impurity lines by their kinematic shift relative to the ^{26}Si lines. This can be seen in Fig. 1 for the ground-state (g.s.) line of ^{10}C.

A. Levels below the proton-emission threshold

Figure 1 shows the ^{26}Si spectra up to the excitation energy of about 5.6 MeV measured at the spectrometer angles −0.3°, 8°, and 17°. The levels used for the energy calibration are indicated by an asterisk. In Fig. 2, we display a blowup of the same ^{26}Si spectra for the excitation-energy region from about 4 to 5.6 MeV.

The energies of the excited states deduced from our measurements in ^{26}Si up to about the proton-emission threshold are listed in the second column of Table II. Previous experimental results are listed in columns 3 to 10. The spin-parity values for the ^{26}Si nucleus, taken from Ref. [27] are listed in the first column of the table.

We resolved two states at 4.8074(25) MeV (2^+) and 4.8287(25) MeV (0^+). The first indications of the existence of a doublet around 4.8 MeV were given by Bohne *et al.* [35], Iliadis *et al.* [19], Caggiano *et al.* [25], and Bardayan *et al.* [22]. Using γ spectroscopy it was found that there are three states at 4.7985(16), 4.8107(29), and 4.8314(21) MeV [27]. Despite the high resolution of 13-keV FWHM in the present experiment we cannot confirm a triplet but observe only the two levels mentioned earlier. These two levels can be observed clearly in the spectrum obtained at the spectrometer angle of −0.3°; see Fig. 2. The level with the lower excitation energy of

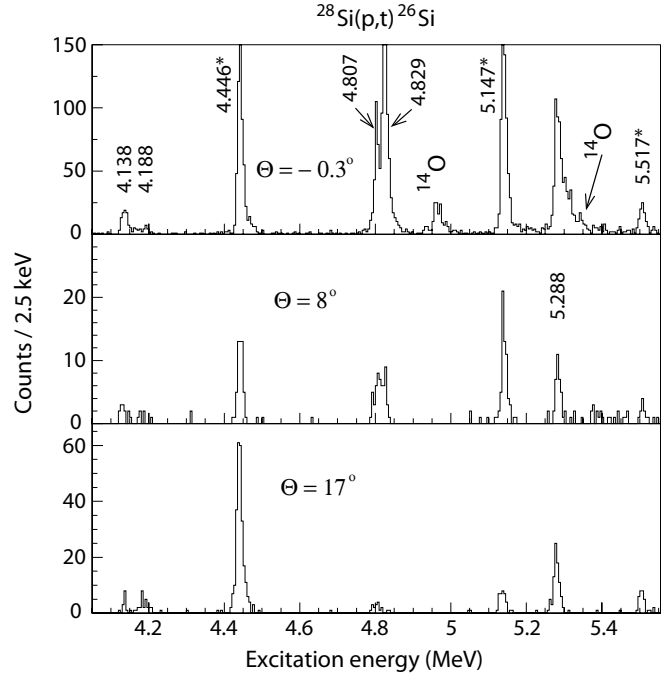

FIG. 2. ^{26}Si spectra in the region of about 4 to 5.6 MeV taken at spectrometer angles −0.3°, 8°, and 17°. The resolved doublet at 4.807 and 4.829 MeV can be seen in the upper panel. The calibration lines are marked with asterisks. The excitation energies determined for ^{26}Si are listed in the second column of Table II.

TABLE II. Levels of ^{26}Si with excitation energies in MeV up to the proton-emission threshold.

J^π adopted[a]	Present (p,t)	Ref. [26] (^{3}He,n)	Ref. [25] (^{3}He,^{6}He)	Ref. [22] (p,t)	Ref. [35] (^{3}He,n)	Ref. [36] (p,t)	Ref. [34][b] (^{3}He,n)	Ref. [27][b] ^{16}O(^{12}C,2$n\gamma$)	Ref. [37] compilation	Shell model[c]	Adopted present[d]
0^+	g.s.[*]	g.s.[e]	g.s.[e]	g.s.[e]	g.s.	g.s.	g.s.	g.s.	g.s.	g.s.	g.s.
2^+	1.7966(8)[*]	1.7959[e]	1.7959[e]	1.7959[e]	1.800(30)	1.795(11)	1.7959(9)	1.7973(8)	1.7959(2)	1.897	1.7967(6)
2^+	2.7850(17)[*]	2.7835[e]	2.7835[e]	2.7835[e]	2.780(30)	2.790(12)	2.7835(18)	2.7864(17)	2.7835(4)	3.007	2.7852(12)
0^+	3.3345(25)[*]	3.3325[e]	–	3.3325[e]	3.330(30)	3.339(19)	3.3325(22)	3.3364(25)	3.3325(3)	3.635	3.3342(17)
3^+	(3.751(4))	3.756[e]	–	3.756[e]	3.760(30)	–	3.756(24)	3.7569(6)	3.756(2)	3.883	3.7568(6)
2^+	4.1383(28)	4.138(4)	4.144(8)	4.155(2)[f]	4.140(30)	–	4.138(17)	4.1393(14)	4.138(1)	4.450	4.1387(10)
3^+	4.188(4)	4.183(4)	4.211(16)	4.155(2)[f]	–	4.183(11)	–	4.1871(14)	4.183(11)	4.317	4.1869(12)
4^+	4.4461(5)[*]	4.446[e]	4.446[e]	4.445[e]	4.450(30)	4.457(13)	4.446(31)	4.4462(5)	4.446(3)	4.365	4.4462(5)
4^+	–	–	–	–	–	–	–	4.7985(16)	–	4.939	4.7985(16)
(2^+)	4.8074(25)	4.806[e]	4.806[e]	4.805[e]	4.810(30)	4.821(13)	4.806(43)	4.8107(29)	4.806(2)	4.883	4.8086(17)
(0^+)	4.8287(25)	–	–	–	–	–	–	4.8314(21)	–	5.034	4.8303(16)
2^+	5.1467(20)[*]	5.145(4)	5.140(10)	5.145(2)	–	–	–	5.1467(20)	–	5.386	5.1457(13)
4^+	5.288(6)	5.291(4)	5.291	5.291(3)	5.310(30)	–	–	5.2882(16)	5.330(20)	5.523	5.2890(13)
4^+	5.5172(16)[*]	5.515(4)	5.526(8)	5.515(5)	–	5.562(28)	–	5.5172(16)	5.562(28)	–	5.5171(14)

[*]Used in the present energy calibration.
[a]J^π values from Ref. [27].
[b]Errors are the sum of the original errors plus the differences of column 4 in Table I as explained in Sec. II.
[c]See Table VI and text for details.
[d]Weighted averages of measured values; energies from compilation by Endt [37] are not included.
[e]Used for calibration in previous experiments.
[f]This level is shown for both adopted levels at 4.1387 and 4.1869 MeV because it cannot be unambiguously attributed to one of these levels.

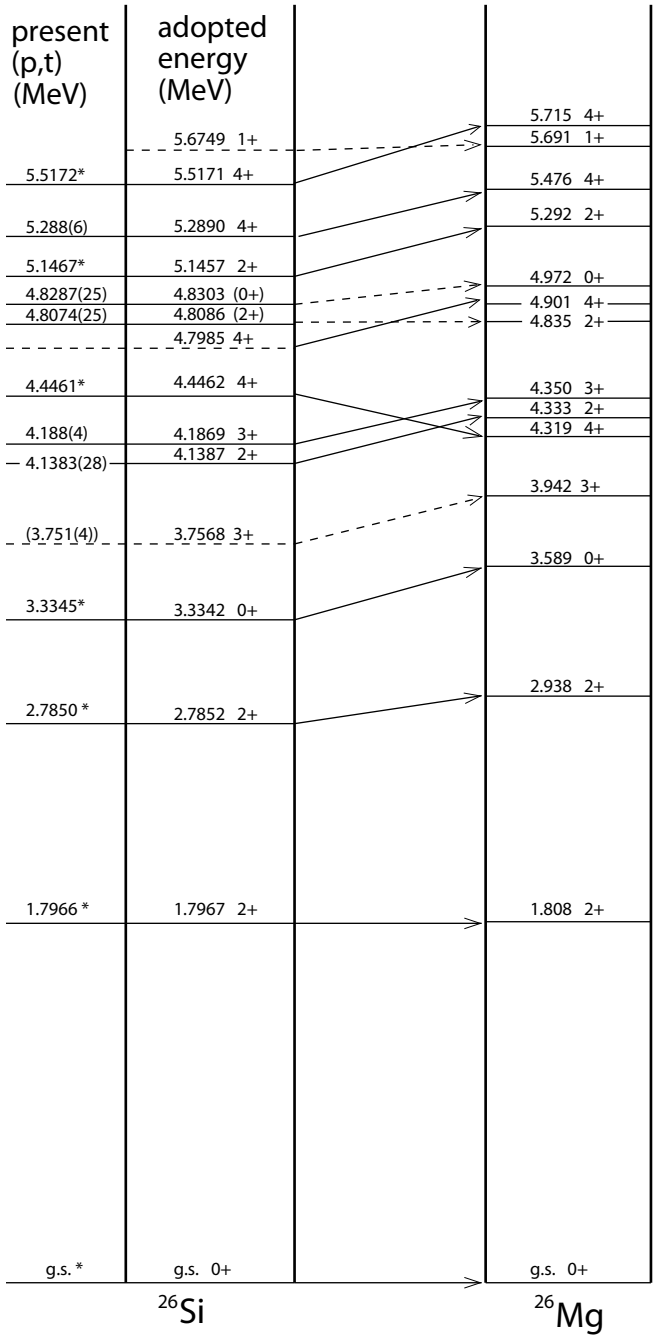

FIG. 3. Possible ^{26}Si mirror assignments for levels below the proton-emission threshold. The ^{26}Mg spin-parity values are taken from Ref. [27]. For notations and details, see Table II.

4.8074(25) MeV can very well correspond to the level measured by Bell *et al.* [34] at 4.806(2) MeV. Possible 0^+, 2^+, and 4^+ spin-parity values were attributed to this doublet in earlier articles [19,22,25,35]. In the mirror spin-parity assignments given in Fig. 3 we adopted the tentative spin-parity suggested by Seweryniak *et al.* [27]: (2^+) and (0^+) for the 4.8074(25) and 4.8287(25) MeV levels, respectively.

The ^{26}Si level measured at an excitation energy of 5.229(12) MeV in the (p,t) experiment by Paddock [36] is not observed in any other study. This includes the (p,t) experiments of Bardayan *et al.* [22,24] as well as the present study. If the 1^+ state at 5.691 MeV in the mirror nucleus ^{26}Mg corresponds to the ^{26}Si 1^+ level at an excitation energy of 5.6749 MeV observed in several studies [25–27], as suggested in Fig. 3, then there is no mirror level in ^{26}Mg corresponding to a 5.229-MeV state in ^{26}Si. Because the resolution in the measurement of Ref. [36] was not better than about 120 keV the level reported at 5.229 MeV is most likely a peak representing the overlap of the 5.1457(13)- and 5.2890(13)-MeV levels obscured by the tail of the ^{10}C$_{g.s.}$ impurity peak at the same position. This level is, therefore, omitted from column 7 in Table II where the levels of Paddock [36] are listed.

B. Levels above the proton threshold

In Fig. 4(a) we show a spectrum measured in the excitation-energy range from 5.5 to 9.2 MeV at the spectrometer angle -0.3°. To evaluate the peaks from ^{12}C and ^{16}O contaminations we also measured, at the same spectrometer setting, a spectrum using a Mylar target shown in Fig. 4(b).

The ^{28}Si spectra measured at all three spectrometer angles are shown in Fig. 5 after the subtraction of the normalized events from the contaminations. The locations of the most prominent contaminant lines are indicated with a "B." The artifacts of this subtraction come from the fact that the Mylar target was thicker than the ^{28}Si targets and the uncertainty of the normalization caused by the burning of two layers of the stacked ^{28}Si target during the experiment. Because of these problems we accepted in our analysis only ^{26}Si levels that are sufficiently strongly populated and clearly separated from the

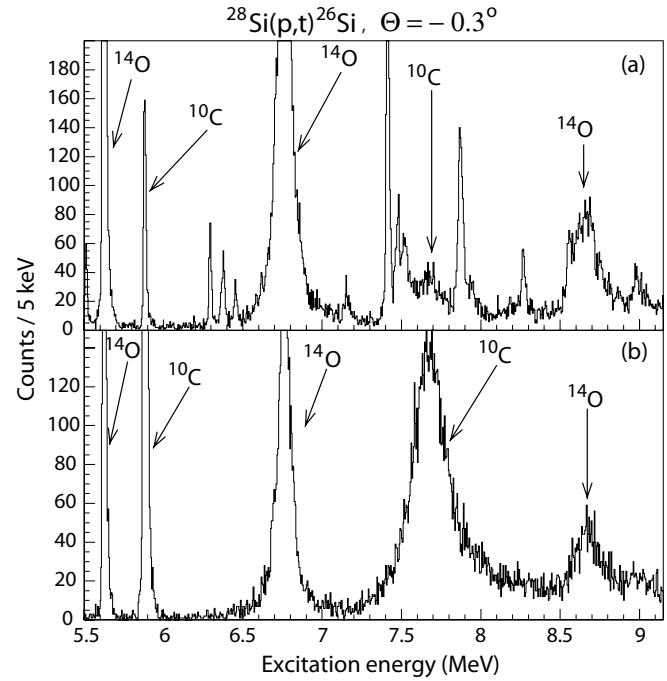

FIG. 4. (a) Triton spectrum at 98.7-MeV incident proton energy on a ^{28}Si target. The ^{14}O and ^{10}C contaminant peaks are labeled. (b) Spectrum using a 1.0 mg/cm^2 Mylar target showing only the ^{14}O and ^{10}C contaminant peaks.

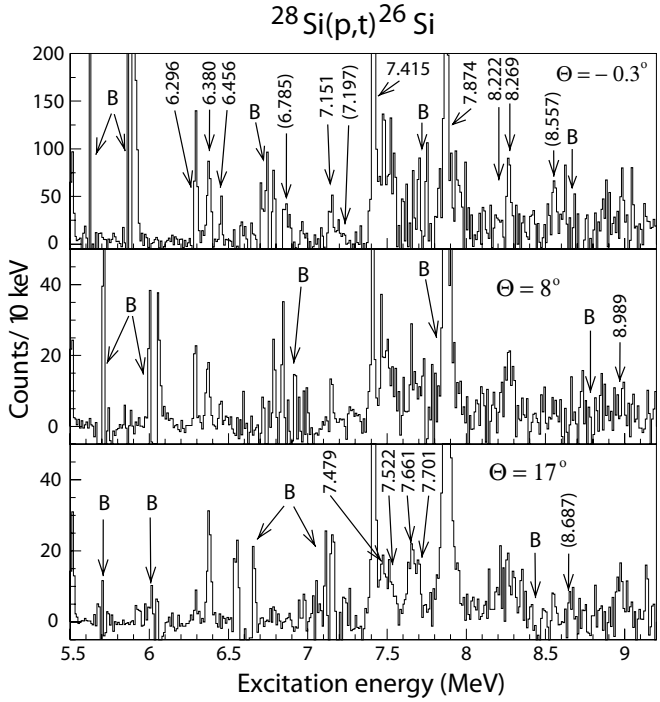

FIG. 5. The ^{28}Si$(p,t)^{26}$Si spectra between the proton-emission threshold and the α-emission threshold taken at spectrometer angles of -0.3°, 8°, and 17°. The excitation energies of the identified ^{26}Si levels are marked in the spectrum where the energies were determined. The remaining parts of the subtraction of ^{10}C and ^{14}O contaminant lines are indicated by a "B." The determined excitation energies for ^{26}Si are listed in the third column of Table III.

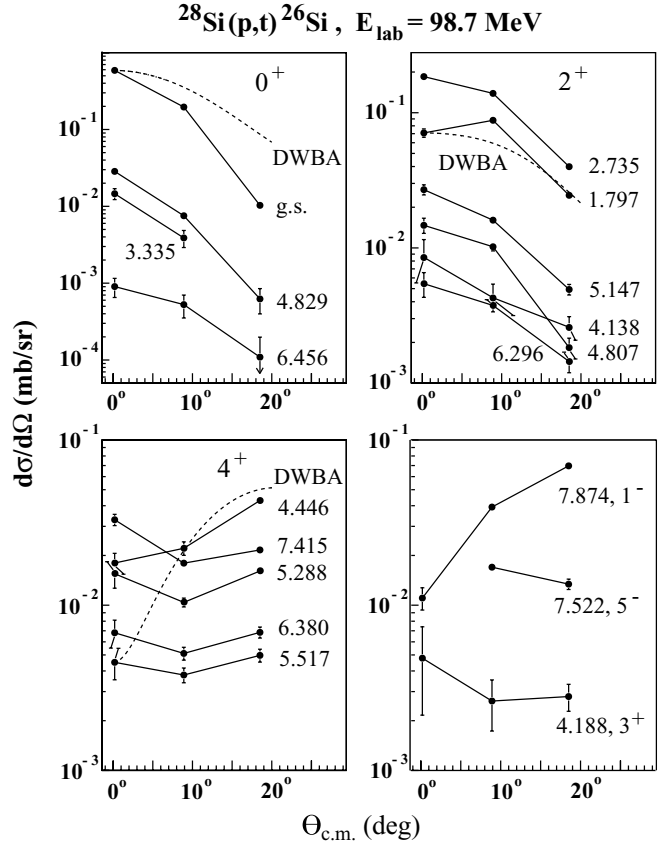

FIG. 6. Cross-section angular distributions of all states where data were measured for at least two angles. The dashed curves are DWBA for selected levels. Note the different y scales for the different panels.

marked background regions and that are clearly visible in at least two spectra. Levels that we observed at one angle only were considered tentative, unless indicated differently, and are shown with excitation energies in parentheses. In Fig. 5, the ^{26}Si levels that we observed between the proton- and the α-emission thresholds are indicated by their excitation energy in the spectrum where their energies were determined.

In Table III we summarize the excitation energies and the spin-parities of all identified proton-unbound states in ^{26}Si that were determined in the present and previous studies. The present excitation energies are listed in column 3. Previous experimental results of excitation energies are listed in columns 4 to 10. The ^{26}Si excitation energies that we used in our stellar rate calculations are listed in the last column. They were calculated as weighted averages of all energies listed in columns 3 to 9. Only data listed by Endt [37] were not taken into account because they are averages of earlier data and, therefore, not independent.

In Table II, we showed that our measured excitation energies below the proton-emission threshold of ^{26}Si are in good agreement with those from previous experiments. However, for the ^{26}Si levels above the proton-emission threshold there are differences between our results and previous results. Owing to our high resolution we identified several new levels that could not be resolved in the early studies by Bohne *et al.* [35] and Paddock [36]. In the more recent studies by Parpottas *et al.* [26] and Bardayan *et al.* [22] listed in columns 4 and 6, most of the levels that we identified were observed, too, but the excitation energies of Ref. [26] often do not agree within their rather small uncertainties of 4 keV for all levels. These differences may be a consequence of the use of the triplet at 4.806 MeV in the energy calibration of Refs. [22,26].

We measured spectra at only three angles but this is sufficient to obtain some information on the transferred angular momentum L as can be seen from Fig. 6. This figure shows the measured cross-section angular distributions of all states where we have data points for at least two angles. We summarize all states with spin-parities of 0^+, 2^+, and 4^+ in the three panels accordingly indicated. The dotted lines represent the results of distorted-wave Born approximation (DWBA) calculations performed with the code DWUCK [39]. The calculated cross sections were normalized to those of the low-lying 0^+, 2^+, and 4^+ states at 0-, 1.7595-, and 5.517-MeV excitation energies, respectively. Details of the DWBA calculations can be found in Ref. [33]. The data as well as the calculations for the $L = 0$ transitions show the typical strong maximum at 0° and a deep first minimum around 20°. Also the $L = 2$ transitions have minima near 20°, but these are less pronounced. The calculated $L = 4$ transitions have maxima around 20° in disagreement with the measured angular distributions that are rather flat. While the general features of the diffraction patterns of the measured and calculated angular distributions

TABLE III. Summary of previous and present spin-parities J^π and excitation energies E_x for levels above the proton-emission threshold (5.5123–9.164 MeV).

J^π [a]	J^π Adopted[b]	Present (p,t)	Ref. [26] (^{3}He,n)	Ref. [25] (^{3}He,^{6}He)	Ref. [22] (p,t)	Ref. [35] (^{3}He,n)	Ref. [36] (p,t)	Ref. [27] ^{16}O(^{12}C,$2n\gamma$)^{26}Si	Ref. [37] Compilation	E_x Adopted[c]
4^+	4^+	5.5172(16)*	5.515(4)	5.526(8)	5.515(5)	–	5.562(28)	5.5172(16)	5.562(28)	5.5171(14)
1^+	1^+	–	5.670(4)	5.678(8)	–	–	–	5.6770(28)	–	5.6749(22)
3^+	3^+	(5.921(12))[d]	5.912(4)	–	5.916(2)	5.910(30)	–	–	–	5.9152(18)
0^+	0^+	(5.944(20))[d]	5.946(4)	5.945(8)	–	–	5.960(22)	–	5.940(25)	5.946(4)
2^+	2^+	6.2957(24)	6.312(4)	–	6.300(4)	6.320(30)	–	–	–	6.3001(18)
2^+	(4^+)	6.3795(29)	6.388(4)	–	6.380(4)	–	6.381(20)	–	6.350(25)	6.3818(20)
0^+	0^+	6.4563(28)	6.471(4)	–	–	6.470(30)	–	–	6.470(30)	6.4611(23)
3^-	3^-	6.785(5)	6.788(4)	–	6.787(4)	6.780(30)	6.786(29)	–	6.789(17)	6.7866(23)
–	$[5^+]$	–	–	–	–	6.880(30)	–	–	6.880(30)	6.88(3)
–	$[3^+]$	–	–	–	7.019(10)	–	–	–	–	7.019(10)
2^+	2^+	7.151(5)	7.152(4)	–	7.160(10)	7.150(30)	7.150(15)	–	7.150(13)	7.1520(28)
–	$[5^+]$	(7.197(8))	–	–	–	–	–	–	–	7.197(8))
0^+	(4^+)	7.4152(23)	7.425(4)	–	7.425(7)	7.390(30)	–	–	7.390(30)	7.4181(19)
2^+	2^+	7.479(12)	7.493(4)	–	7.498(4)	7.480(30)	7.476(20)	–	7.489(15)	7.4942(27)
–	$[5^-]$	7.522(12)	–	–	–	–	–	–	–	7.522(12)
–	$[2^+]$	7.661(12)	–	–	–	–	–	–	–	7.661(13)
3^-	3^-	7.701(12)	7.694(4)	–	7.687(22)	–	7.695(30)	–	7.695(30)	7.695(4)
1^-	1^-	7.874(4)	7.899(4)	–	7.900(22)	7.900(30)	7.902(21)	–	7.892(15)	7.8839(24)
–	$[3^+]$	–	–	–	–	8.120(30)	–	–	8.120(20)	8.12(3)
	$[1^-]$	8.222(5)	–	–	–	–	–	–	–	8.222(5)
–	$[2^+]$	8.269(4)	–	–	–	–	–	–	–	8.269(4)
–	$[2^+]$	(8.557(4))	–	–	–	–	–	–	–	(8.557(4))
–	$[4^+]$	(8.687(12))	–	–	–	8.700(30)	–	–	–	8.689(11)
–	$[4^+]$	8.989(7)	–	–	–	–	–	–	–	8.989(7)

[a] J^π values from Ref. [26].
[b] Mirror assignments in brackets as defined in Fig. 7.
[c] Weighted average, only E_x compiled by Endt [37] are excluded; see text.
[d] Tentative E_x excluded from the averaging process.

are similar, the quantitative agreement is insufficient to allow unambiguous spin assignments for $L > 2$. This is the reason why our (4^+) assignments are tentative for the 6.3795- and 7.4152-MeV levels based on the comparison with measured angular distributions of the known 4^+ levels at 4.446, 5.288, and 5.517 MeV shown in Fig. 6.

While we did not use the DWBA analysis in this work to make any new spin-parity assignments, the agreement of measured and calculated angular distributions may suggest that such a comparison may be useful for the determination of the lower angular momenta $L = 0$ and $L = 2$. However, this procedure neglects possible multistep procedures that may be present in particular at lower incident beam energies and can lead to erroneous conclusions. As an example Bardayan *et al.* [24] have shown that measured angular distributions with limited angular range of the state at 5.914 MeV in ^{26}Si may be explained by assuming a 0^+ as well as a 3^+ spin-parity.

The spin-parities in the first column of Table III are from Ref. [26]. Those listed in column 2 were adopted to be used in our stellar rate calculations. In that, we accepted all of the spin-parity assignments made in Ref. [26] except for the spins of the 6.3795- and 7.415-MeV levels as mentioned previously. Where no spin-parities were known we made mirror assignments as defined by dashed lines in Fig. 7. To indicate that these assignments are assumptions, rather than based on measurements, they are shown in brackets in Table III and throughout the article.

The level with an adopted energy of 5.6749(22) MeV (last column of Table III) was assigned a spin-parity of 1^+ in Refs. [25–27]. This level was not observed in the present experiment or in previous (p,t) experiments [22,36] that were selective for natural parity levels. Therefore, we adopted an unnatural 1^+ spin-parity for this state and related it to the 1^+ state at 5.691 MeV in the mirror nucleus ^{26}Mg as shown in Fig. 7.

A doublet of two states near 5.912(4) and 5.946(4) MeV has been observed in previous experiments [22,26,35]. Initially the level at 5.921(12) MeV was assigned 0^+ spin-parity based on a DWBA analysis in Ref. [22] while the state at 5.942(20) MeV was assigned a spin-parity of 3^+ based on a comparison with the level structure of the mirror nucleus by Caggiano *et al.* [25]. A subsequent, more detailed study of ^{28}Si$(p,t)^{26}$Si populating the states in this excitation range [24] suggests a 3^+ assignment for the state at 5.921 MeV, supporting the analysis of the ^{24}Mg(^{3}He,n)^{26}Si two-proton stripping reaction by Parpottas *et al.* [26]. The latter article also suggests a 0^+ assignment for the state at 5.944 MeV, which would characterize it as the mirror level to the 0^+ state at 6.256 MeV in ^{26}Mg. These spin assignments were subsequently confirmed by the analysis [21] of recent β-delayed

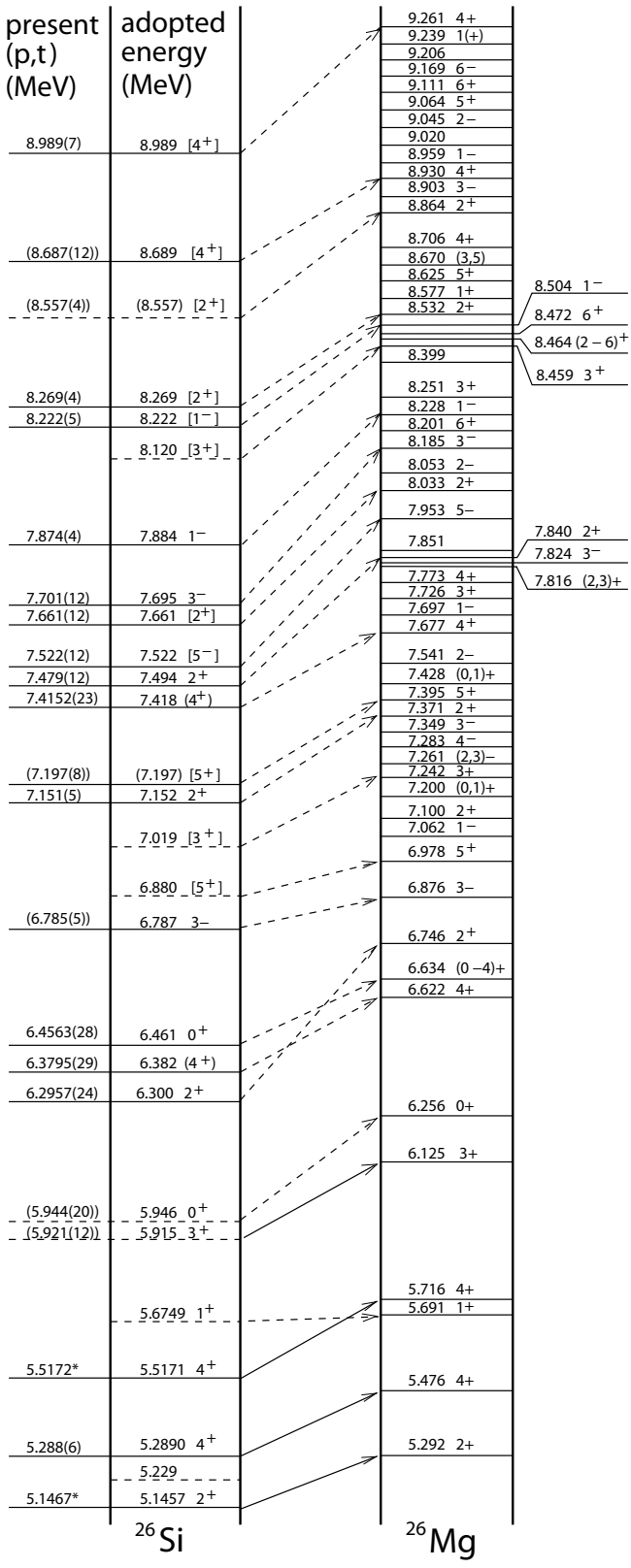

FIG. 7. The possible ^{26}Si mirror assignments for levels above the proton-emission threshold. The ^{26}Mg spin-parity values are from Ref. [38]. The ^{26}Si adopted energies are taken from the last column of Table III.

proton and γ-decay studies of ^{26}P [40] and are also consistent with the results of the ^{25}Al$(d,n)^{26}$Si transfer measurement [28]. In the present experiment, we were not able to observe these two levels at the two forward angles because of contamination by a ^{10}C impurity line. At a spectrometer angle of 17° the peaks are weak and the statistics does not allow us to make any conclusive decision on the spin assignment. We therefore adopt the assignment made by Bardayan *et al.* [24] and Wrede [21].

Three levels at 6.2957(24) MeV 2^+, 6.3795(29) MeV (4^+), and 6.4563(28) MeV 0^+ are clearly observed at all three measured scattering angles with the exception of the state at 6.4563 MeV that does not rise above background at the most backward angle of 17°. The deduced excitation energies are in agreement with Refs. [22,35,36] but not with Ref. [26]. The excitation energies quoted in the latter work are systematically 8–16 keV higher. This discrepancy might be attributed to the use of the unresolved triplet near 4.806 MeV for their calibrations as mentioned above earlier. Our present spin and parity assignment of the state at 6.3795 MeV is based on the angular distributions shown in Fig. 6. The tentative $J^\pi = (4^+)$ assignment for this level disagrees with the assignment made by Parpottas *et al.* [26] but is consistent with the assignment made on the basis of β-delayed proton studies by Thomas *et al.* [40].

Because of the strong ^{14}O contaminant peak obscuring the excitation range around 7 MeV we could not determine if the previously observed levels at 6.880 and 7.019 MeV were excited in our measurement. In the excitation energy range from 6.785 and 7.479 MeV we observe five energy levels. Based on a weak peak structure observed at the forward angle we tentatively propose a level at 7.197 MeV. In the corresponding excitation energy range the mirror nucleus ^{26}Mg shows a considerably larger number of levels preventing unanimous spin assignments. Our tentative (4^+) assignment for the 7.415-MeV state is based on the observed angular distribution shown in Fig. 6. The assignments for the other states are tentative, based on excitation energy and the fact that (p,t) two-neutron transfer reactions populate selectively natural-parity levels. The five observed levels and the suggested spin-parity assignments are listed in Table III.

At higher excitation energies we observe clearly two states at 7.522(12) MeV $[5^-]$ and 7.661(12) MeV $[2^+]$ that were not observed beforehand. The 12-keV uncertainty in the excitation energy is caused by the larger than normal uncertainty at the 17° spectrometer angle due to kinematic broadening. These two levels are not clearly observed at −0.3° and 8° spectrometer angles because at those angles they overlap with a broad ^{10}C resonance. We confirm the previously observed levels at 7.701(12) and 7.874(4) MeV previously measured in several studies as shown in Table III. For these two states we adopt the spin and parity assignments by Parpottas *et al.* [26] and Bardayan *et al.* [22]. We do not observe the 3^+ level at 8.120 MeV which has been reported in earlier (^{3}He,n) reaction studies [35,37].

At higher energies near the α threshold we identified five levels at 8.222(5), 8.269(4), (8.557(4)), (8.687(12)), and

8.989(7) MeV. These levels are observed for the first time except for a level at 8.700(30) that was seen in a ^{24}Mg(^{3}He,n) study of Ref. [35]. Three of the levels can be seen at all three spectrometer angle settings while the two remaining ones could only be seen at one angle because of background impurities. The suggested spin and parity assignments are therefore only tentative.

IV. ASTROPHYSICAL IMPLICATIONS FOR THE ^{25}Al(p,γ)^{26}Si REACTION

The total reaction rate for ^{25}Al$(p,\gamma)^{26}$Si can be expressed as the sum of individual narrow resonances corresponding to the unbound states in ^{26}Si and the nonresonant direct capture to bound states in ^{26}Si [17,19]. The resonances are very narrow because of the Coulomb and centrifugal (in case of the single-particle orbit angular momentum $\ell \neq 0$) barriers reducing the proton widths Γ_p. Therefore, a single-resonance formalism [41] can be applied to describe the resonant contribution to the reaction rate,

$$N_A\langle\sigma\upsilon\rangle_{\rm res} = 1.54\times10^5(\mu T_9)^{-3/2}\sum_i(\omega\gamma)_i \times\exp(-11.605E_i/T_9)[{\rm cm^3\,s^{-1}\,mol^{-1}}], \quad (1)$$

with μ being the reduced mass of the target and projectile in units of amu, GK the temperature in units of GK, $(\omega\gamma)_i$ the strength in units of eV, and E_i the energy of the ith resonance in units of MeV.

One important difference between the results of the present calculations and those done previously [25,26] is a new value for the proton-emission threshold for ^{26}Si [23]. Instead of the value previously used (5.518 MeV), the new ^{26}Si proton-emission threshold value is 5.5123(10) MeV. This translates into a change of the actual values of the resonance energies E_i used for calculating the reaction rate.

Due to this shift the 5.5171(14)-MeV level is located above the ^{26}Si proton-emission threshold. However, its 0.0048-MeV resonance energy is well below the Gamow window for the ^{25}Al$(p,\gamma)^{26}$Si reaction for temperatures above 0.01 GK. Therefore, we do not consider this level in our reaction-rate calculations.

The resonance strength $\omega\gamma$ for levels with a spin of J is directly correlated with the proton partial width Γ_p and the γ partial width Γ_γ of the unbound level:

$$\omega\gamma = \frac{2J+1}{12}\frac{\Gamma_p\Gamma_\gamma}{\Gamma_{\rm tot}}. \quad (2)$$

The total width $\Gamma_{\rm tot}$ represents the sum of the two partial widths.

The proton partial decay width is given by

$$\Gamma_p = C^2S\cdot\Gamma_p^{\rm sp}, \quad (3)$$

where C^2S is the single-particle spectroscopic factor and $\Gamma_p^{\rm sp}$ is the single-particle width.

The single-particle width $\Gamma_p^{\rm sp}$ has been calculated in a Woods-Saxon potential with a radius of $R = 3.68$ fm and a diffuseness of $a = 0.6$ fm using the code DWUCK4 [39]. The proton partial widths Γ_p are calculated using Eq. (3)

TABLE IV. Resonance energies and predictions of single-particle spectroscopic factors for unbound states in $A = 26$, $T = 1$ systems.

E_x[a] (MeV)	$E_{\rm res}$ (MeV)	J^π[b] Mirror	C^2S [19]	C^2S present work
5.6749	0.1626	1^+	0.004	0.0048
5.9152	0.4029	3^+	0.14	0.141
5.9460	0.4339	0^+	0.047	0.039
6.3001	0.7878	2^+	0.028	0.0087
6.3818	0.8695	$[4^+]$	0.0089	0.015
6.4611	0.9488	0^+		0.039
6.7866	1.2743	3^-		
6.8800	1.3677	$[5^+]$		0.0145
7.0190	1.5067	$[3^+]$		0.0039
7.1520	1.6397	2^+		0.045
7.1970	1.6849	$[5^+]$		0.0102

[a] ^{26}Si excitation energies are taken from last column in Table III.
[b] J^π values without brackets are taken from Ref. [26]. J^π values within brackets are obtained by the mirror assignments given in Fig. 7.

on the basis of the single-particle spectroscopic factors C^2S calculated for sd-shell levels in ^{26}Si, as shown in the last column of Table IV. These calculations are based on the USDA interaction [42]. There is good agreement with the spectroscopic factors of Iliadis *et al.* [19] for the three lowest-lying states. Table V lists the observed levels in ^{26}Si above

TABLE V. Resonance energies, spin-parities, and resonance strengths used in the rate calculations of the ^{25}Al$(p,\gamma)^{26}$Si reaction.

E_x[a] (MeV)	$E_{\rm res}$ (MeV)	J^π[b] Mirror	Γ_p (eV)	Γ_γ Mirror (eV)	$\omega\gamma$ (eV)
5.6749	0.1626	1^+	8.39×10^{-9}	1.10×10^{-1}[c]	2.10×10^{-9}
5.9152	0.4029	3^+	3.46	4.31×10^{-2}[d]	2.48×10^{-2}
5.9460	0.4339	0^+	1.72×10^{-2}	8.34×10^{-3}[d]	4.68×10^{-4}
6.3001	0.7878	2^+	4.46×10^{1}	2.65×10^{-2}[d]	1.10×10^{-2}
6.3818	0.8695	$[4^+]$	0.545	2.47×10^{-2}[d]	1.77×10^{-2}
6.4611	0.9488	0^+	9.28×10^{2}	9.08×10^{-2}[d]	7.56×10^{-3}
6.7866	1.2743	3^-	1.77×10^{2}[e]	7.41×10^{-3}[d]	4.32×10^{-3}
6.8800	1.3677	$[5^+]$	3.94×10^{1}	5.09×10^{-2}[d]	4.66×10^{-2}
7.0190	1.5067	$[3^+]$	7.25×10^{2}	7.78×10^{-2}[d]	4.54×10^{-2}
7.1520	1.6397	2^+	1.24×10^{4}	1.00×10^{-2}[f]	4.17×10^{-3}
7.1970	1.6849	$[5^+]$	1.04×10^{2}	4.36×10^{-2}[d]	4.00×10^{-2}
7.4181	1.9058	(4^+)	–	1.00×10^{-2}[f]	7.50×10^{-3}
7.4942	1.9819	2^+	–	1.00×10^{-2}[f]	4.17×10^{-3}
7.5220	2.0099	$[5^-]$	–	2.25×10^{-2}[d]	2.07×10^{-2}
7.6610	2.1486	$[2^+]$	–	1.00×10^{-2}[f]	4.17×10^{-3}
7.6950	2.1823	3^-	–	1.00×10^{-2}[f]	5.83×10^{-3}
7.8839	2.3716	1^-	–	5.17×10^{-1}[d]	1.29×10^{-1}
8.1200	2.6077	$[3^+]$	1.8×10^{-2}[e]	1.00×10^{-2}[f]	3.75×10^{-3}

[a] ^{26}Si excitation energies are taken from the last column in Table III.
[b] J^π values without brackets are taken from Ref. [26]. J^π values within brackets are obtained by the mirror assignments given in Fig. 7.
[c] Theoretically calculated Γ_γ value, taken from Ref. [42].
[d] Γ_γ values calculated from the half-life data for ^{26}Mg mirror levels [38].
[e] Single-particle spectroscopic factor adopted to be 0.01.
[f] A constant value of 0.01 eV is assumed for Γ_γ.

the proton-emission threshold with their proton and γ partial decay widths as well as with the resulting resonance strengths.

For the γ partial widths Γ_γ of the levels marked by the superscript d, we adopted the known γ-decay lifetimes of the mirror states in ^{26}Mg [38]. The energy dependence of Γ_γ is given as

$$\Gamma_\gamma(E_\gamma) = \alpha_L E_\gamma^{2L+1}, \quad (4)$$

where L is the multipolarity of the emitted γ ray and α_L corresponds to the transition strengths that should be identical for mirror transitions. For the levels indicated by the superscript g we adopted a constant Γ_γ value of 0.01 eV, because there are no experimental or theoretical data available. For the 0.1626(22)-MeV 1^+ resonance the theoretically calculated [42] Γ_γ value is used, because the experimental value has only a lower limit [38] of 0.08 eV.

We have calculated the resonant reaction-rate component for ^{25}Al$(p,\gamma)^{26}$Si based on the adopted ^{26}Si excitation energies (Table III) and the resonance strengths listed in Table V.

The nonresonant direct-capture contribution (DC) to the reaction rate [41] corresponds directly to the total astrophysical S factor by summing over the single-particle contributions $S(E_0)_i$ from all direct transitions to the bound states in ^{26}Si and is given by

$$N_A\langle\sigma\upsilon\rangle_{\rm DC} = 1.86\times10^7(T_9)^{-2/3}\sum_i S(E_0)_i \times \exp\left(-23.195/T_9^{1/3}\right)[\mathrm{cm^3\,s^{-1}\,mol^{-1}}], \quad (5)$$

with T_9 the temperature in GK and $S(E_0)_i$ in units of keV-barn.

The shell-model information together with the calculated S-factors $S(E_0)_i$ used in the DC calculations is summarized in Table VI. E_f is the adopted excitation energy for the final bound state from Table II, and $E_{\rm sm}$ is the excitation energy of the corresponding level of the shell model calculation. J_f is the spin of the final state, l_f is the orbital momentum of the final bound state, and l_i is the orbital angular momentum of the initial free-particle wave. The total S factor $S(E_0) = \sum_i S(E_0)_i$ is calculated in the framework of the Wood-Saxon potential model as outlined in previous works [17,19]. The original estimate of the direct-capture component [17] includes only the ground state and the first two excited states. In a subsequent analysis, transitions to all 13 bound states have been included in the calculation of the total S factor. This increased the total value of the S factor to $S(E_0) = 27$ keV-b [19]. The single-particle spectroscopic factors for the final state were adopted from shell-model calculations that show good agreement with the experimentally known single-particle spectroscopic factors of the mirror levels in ^{26}Mg. The calculations presented here take into account the 5-keV reduction of the ^{25}Al$(p,\gamma)^{26}$Si Q value to $Q = 5.5123$ MeV [23] and are based on new spectroscopic factors calculated for sd-shell levels in ^{26}Si using the USDA interaction [42]. We obtain a total DC S factor of 28 keV-b, a slightly larger value than the previous result [19].

TABLE VI. Spectroscopic information used in the direct-capture (DC) rate calculations of the ^{25}Al$(p,\gamma)^{26}$Si reaction. For definitions, see text.

E_f (MeV)	$E_{\rm sm}$ (MeV)	J_f	l_f	l_i	Shell model configuration	C^2S	$S(E_0)_i$ (keV-b)
0	0	0	2	1	$1d5/2$	2.4701	1.32
1.7967	1.897	2	0	1	$2s1/2$	0.0341	0.75
		2	2	1	$1d5/2d3/2$	0.3633	0.77
2.7852	3.008	2	0	1	$1s1/2$	0.4633	10.16
		2	2	1	$1d5/2d3/2$	0.0801	0.14
3.3342	3.635	0	2	1	$1d5/2$	0.2319	0.07
3.7568	3.883	3	0	1	$2s1/2$	0.2726	8.64
		3	2	1	$1d5/2d3/2$	0.2718	0.06
4.1387	4.45	2	0	1	$2s1/2$	0.0234	1.21
		2	2	1	$1d5/2d3/2$	0.0522	0.06
4.1869	4.317	3	0	1	$2s1/2$	0.0697	2.3
		3	2	1	$1d5/2d3/2$	0.0674	0.11
4.4462	4.365	4	2	1	$1d5/2d3/2$	0.0845	0.163
4.7985	4.939	4	2	1	$1d5/2d3/2$	0.1293	0.211
4.8086	4.883	2	0	1	$2s1/2$	0.042	1.14
		2	2	1	$1d5/2d3/2$	0.0439	0.04
4.8303	5.034	0	2	1	$2s1/2$	0.0395	0.01
5.1457	5.386	2	0	1	$2s1/2$	0.0139	0.44
		2	2	1	$1d5/2d3/2$	0.4521	0.31
5.2890	5.523	4	2	1	$1d5/2d3/2$	0.1916	0.194

On basis of the data presented in Tables V and VI, we have computed new ^{25}Al$(p,\gamma)^{26}$Si reaction rates summarized in Table VII. The contributions of the critical low-energy resonances and the direct capture are presented in Fig. 8. The direct capture clearly determines the low-temperature rate corresponding to stellar hydrogen-burning conditions. At these temperatures the rate is too small to compete with the ^{26}Al β^+ decay and therefore has no relevance for the reaction path. At higher temperatures in excess of 0.05 GK as anticipated for explosive hydrogen burning in novae or x-ray burst environments, the reaction rate is dominated by the resonant contributions. This is, namely, the resonance at 163 keV, $J^\pi = 1^+$, which characterizes the rate under the temperature conditions of nova burning up to 0.2 GK. For temperatures 0.2 to 2.0 GK, characteristic for explosive hydrogen-burning conditions on accreting neutron stars, the rate is dominated by the $J^\pi =^+$ resonance at 403-keV resonance energy. At higher temperatures (5–10 GK), resonances between 800- and 1600-keV proton energy dominate the reaction rate.

In Fig. 9 we show the total ^{25}Al$(p,\gamma)^{26}$Si reaction rates in comparison with those computed by Wiescher *et al.* [17], Iliadis *et al.* [19], Wrede [21], Caggiano *et al.* [25], and Parpottas *et al.* [26]. Also shown for comparison is the reaction-rate prediction based on the statistical model [Hauser-Feshbach (HF)] using the code CIGAR (Ref. [43]). The results are in good agreement with predictions of the HF codes NON-SMOKER [44] and TALYS [45]. At low tempertures ($\leqslant$0.2 GK), the statistical model (HF) is not applicable because of the low-level density in that excitation range in ^{26}Si. Table VII contains the numerical values of the direct capture, the resonant reaction rate, and the total reaction rates. All rate predictions agree well within a factor of 3 to 10 with the exception of rates below 0.2 GK, where larger deviations occur in the calculations of Refs. [17] and [19]. The differences are mainly due to spin assignments and the choice of specific spectroscopic factors.

TABLE VII. Calculated rates $N_A\langle\sigma\upsilon\rangle$ of the ^{25}Al$(p,\gamma)^{26}$Si reaction as a function of temperature (Temp.) in units of GK for the direct capture (DC), the resonances (RES), and the sum of both (Total). Also shown for comparison are the reaction rates using the statistical model (HF). The reaction rates are given in units of cm^3 mol^{-1} s^{-1}.

Temp.	$N_A\langle\sigma\upsilon\rangle_{\rm DC}$	$N_A\langle\sigma\upsilon\rangle_{\rm RES}$	$N_A\langle\sigma\upsilon\rangle_{\rm Total}$	$N_A\langle\sigma\upsilon\rangle_{\rm HF}$
0.01	1.57×10^{-37}	3.69×10^{-83}	1.57×10^{-37}	2.97×10^{-33}
0.02	4.37×10^{-28}	1.26×10^{-42}	4.37×10^{-28}	3.18×10^{-23}
0.03	1.64×10^{-23}	3.14×10^{-29}	1.64×10^{-23}	1.25×10^{-18}
0.04	1.25×10^{-20}	1.38×10^{-22}	1.26×10^{-20}	9.23×10^{-16}
0.05	1.39×10^{-18}	1.24×10^{-18}	2.63×10^{-18}	1.01×10^{-13}
0.06	5.04×10^{-17}	5.08×10^{-16}	5.59×10^{-16}	3.68×10^{-12}
0.07	8.84×10^{-16}	3.61×10^{-14}	3.70×10^{-14}	6.49×10^{-11}
0.08	9.37×10^{-15}	8.59×10^{-13}	8.69×10^{-13}	6.94×10^{-10}
0.09	6.88×10^{-14}	9.91×10^{-12}	9.97×10^{-12}	5.14×10^{-9}
0.1	3.83×10^{-13}	6.89×10^{-11}	6.92×10^{-11}	2.87×10^{-8}
0.15	1.62×10^{-10}	2.23×10^{-08}	2.24×10^{-08}	1.18×10^{-5}
0.2	7.24×10^{-09}	3.51×10^{-06}	3.52×10^{-06}	4.72×10^{-4}
0.3	8.31×10^{-07}	4.24×10^{-03}	4.24×10^{-03}	3.79×10^{-2}
0.4	1.63×10^{-05}	1.36×10^{-01}	1.36×10^{-01}	0.482
0.5	1.34×10^{-04}	$1.01 \times 10^{+00}$	$1.01 \times 10^{+00}$	2.546
0.6	6.66×10^{-04}	$3.64 \times 10^{+00}$	$3.65 \times 10^{+00}$	8.10
0.7	2.38×10^{-03}	$8.82 \times 10^{+00}$	$8.82 \times 10^{+00}$	1.93×10^{1}
0.8	6.79×10^{-03}	$1.67 \times 10^{+01}$	$1.67 \times 10^{+01}$	3.77×10^{1}
0.9	1.64×10^{-02}	$2.68 \times 10^{+01}$	$2.68 \times 10^{+01}$	6.44×10^{1}
1.0	3.51×10^{-02}	$3.87 \times 10^{+01}$	$3.87 \times 10^{+01}$	9.96×10^{1}
1.5	5.03×10^{-01}	$1.04 \times 10^{+02}$	$1.04 \times 10^{+02}$	3.89×10^{2}
2.0	$2.65 \times 10^{+00}$	$1.57 \times 10^{+02}$	$1.60 \times 10^{+02}$	7.95×10^{2}
3.0	$2.07 \times 10^{+01}$	$2.25 \times 10^{+02}$	$2.27 \times 10^{+02}$	1.68×10^{3}
4.0	$7.44 \times 10^{+01}$	$2.66 \times 10^{+02}$	$3.41 \times 10^{+02}$	2.50×10^{3}
5.0	$1.83 \times 10^{+02}$	$2.96 \times 10^{+02}$	$4.79 \times 10^{+02}$	3.20×10^{3}
6.0	$3.60 \times 10^{+02}$	$3.17 \times 10^{+02}$	$6.77 \times 10^{+02}$	3.80×10^{3}
7.0	$6.16 \times 10^{+02}$	$3.32 \times 10^{+02}$	$9.48 \times 10^{+02}$	4.33×10^{3}
8.0	$9.55 \times 10^{+02}$	$3.40 \times 10^{+02}$	$1.29 \times 10^{+03}$	4.80×10^{3}
9.0	$1.38 \times 10^{+03}$	$3.43 \times 10^{+02}$	$1.72 \times 10^{+03}$	5.25×10^{3}
10.0	$1.89 \times 10^{+03}$	$3.43 \times 10^{+02}$	$2.23 \times 10^{+03}$	5.71×10^{3}

Also shown in Fig. 9 is the β-decay rate $N_A\langle\beta\rangle$ given by

$$N_A\langle\beta\rangle = \frac{A}{x_H \rho t_{1/2}} \tag{6}$$

of ^{25}Al converted to the same units as the reaction rates. The decay rates are shown for two density assumptions: $\rho = 10^3$ g/cm^3, typical for novae, and $\rho = 10^6$ g/cm^3, typical for x-ray burst environments. $A = 1$ is the atomic number for hydrogen in units of g/mol and $x_H = 0.5$ is the adopted mass fraction for hydrogen. The resulting rates of $N_A\langle\sigma\upsilon\rangle = 2.79 \times 10^{-4}$ cm^3 mol^{-1} s^{-1} and 2.79×10^{-7} cm^3 mol^{-1} s^{-1}, respectively, are shown as horizontal lines. The ^{25}Al$(p,\gamma)^{26}$Si reaction becomes effective under the temperature-density conditions with $N_A\langle\sigma\upsilon\rangle \geqslant N_A\langle\beta\rangle$. Based on the results presented here, this takes place at 0.28 GK in novae burning and at 0.184 GK under x-ray burst conditions.

One of the remaining uncertainties is the spin assignment for the two states at 403 keV (3^+) and 434 keV (0^+), for which we followed the suggestions of previous work [24,26]. Previous work had suggested a reverse assignment of 403 keV

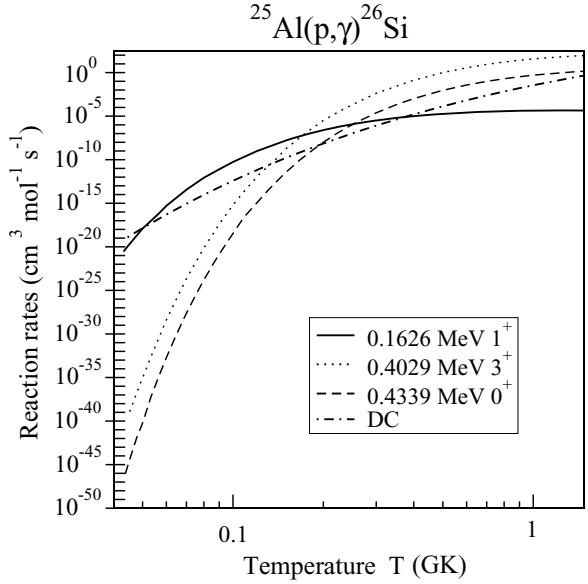

FIG. 8. The contributions of the first three resonances above the proton-emission threshold to the ^{25}Al$(p,\gamma)^{26}$Si reaction rates.

(0^+) and 434 keV (3^+) as discussed earlier. Because both states are fairly close in excitation energy, a change of spin results only in a relatively small change of reaction rate. Adopting the present assignment enhances the rate in the temperature range of 0.2 to 1.5 GK by a factor of 2. This is well within the order of the overall uncertainty of the reaction rate. At temperatures above 1 GK the resonant component of the reaction rate suggested by the present analysis is only slightly

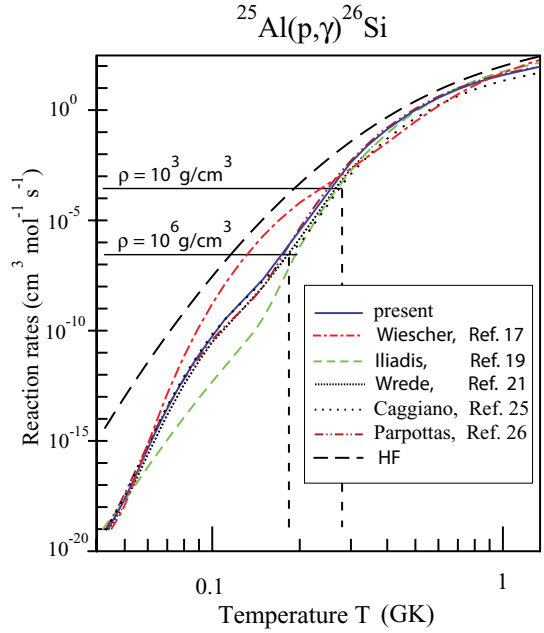

FIG. 9. (Color online) The ^{25}Al$(p,\gamma)^{26}$Si reaction rates as a function of temperature. The labeled curves indicate reaction rates calculated in Refs. [17,19,21,25,26]. The constant lines indicate the decay rates for ^{25}Al calculated for densities of $\rho = 10^3$ and 10^6 g/cm^3 in the hydrogen-burning environment. For details, see text.

lower than the HF predictions. This difference is associated with the fact that not all of the unbound states in ^{26}Si have been observed in the present experiment. Figure 7 does indeed show about three times as many states in the mirror nucleus ^{26}Mg at excitation energies above 7 MeV than observed in the ^{28}Si$(p,t)^{26}$Si reaction. This suggests that the resonant component at higher temperatures, $\geqslant$1 GK, should be larger than quoted in Table VII. Therefore, we suggest to adopt the statistical (HF) rate for application in that temperature range.

All these results indicate that the reaction rate of ^{25}Al$(p,\gamma)^{26}$Si is fairly well consolidated. The remaining uncertainty depends primarily on the choice of spin assignment and the theoretical predictions for the single-particle strengths of the resonance states. Nevertheless, these predictions need to be verified by either single-particle transfer measurements or radiative-capture measurements. The measurement of transfer reactions with radioactive ^{25}Al beams [28] has been the first step. Improved beam intensities are necessary for testing directly the predictions based on indirect studies such as the one presented in this work.

ACKNOWLEDGMENTS

This work was supported by the National Science Foundation under Grant No. PHY01-40324 and by the Joint Institute for Nuclear Astrophysics, NSF-PFC, under Grant No. PHY02-16783. H.S. is supported by NSF Grant No. PHY06-06007. B.A.B. is supported by NSF Grant No. PHY-0758099.

[1] T. Lee, D. A. Papanastassiou, and G. J. Wasserburg, Astrophys. J. Lett. **211**, L107 (1977).
[2] T. Lee, D. A. Papanastassiou, and G. J. Wasserburg, Astrophys. J. Lett. **220**, L21 (1978).
[3] J. W. Truran and A. G. W. Cameron, Astrophys. J. **219**, 226 (1978).
[4] W. D. Arnett and J. P. Wefel, Astrophys. J. Lett. **224**, L139 (1978).
[5] M. Arnould, H. Nørgaard, F.-K. Thielemann, and W. Hillebrandt, Astrophys. J. **237**, 931 (1980).
[6] F.-K. Thielemann and W. Hillebrandt, Astrophys. J. **255**, 617 (1982).
[7] D. D. Clayton and L. Jin, Astrophys. J. Lett. **451**, L87 (1995).
[8] W. A. Mahoney, J. C. Ling, A. S. Jacobson, and R. Lingenfelter, Astrophys. J. **262**, 742 (1982).
[9] R. Diehl *et al.*, Astron. Astrophys. **298**, 445 (1995).
[10] N. Prantzos and M. Cassé, Astrophys. J. **307**, 324 (1986).
[11] N. Prantzos and R. Diehl, Phys. Rep. **267**, 1 (1996).
[12] M. Forestini, G. Paulus, and M. Arnould, Astron. Astrophys. **252**, 597 (1991).
[13] M. Limongi and A. Chieffi, Astrophys. J. **647**, 483 (2006).
[14] J. Jose, A. Coc, and M. Hernanz, Astrophys. J. **520**, 347 (1999).
[15] M. Mowlavi and M. Arnould, Astron. Astrophys. **361**, 959 (2000).
[16] A. Chieffi and M. Limongi, Mem. Soc. Astron. Ital. **78**, 538 (2007).
[17] M. Wiescher, J. Görres, F.-K. Thielemann, and H. Ritter, Astron. Astrophys. **160**, 56 (1986).
[18] C. M. Deibel, J. A. Clark, R. Lewis, A. Parikh, P. D. Parker, and C. Wrede, Phys. Rev. C **80**, 035806 (2009).
[19] C. Iliadis, L. Buchmann, P. M. Endt, H. Herndl, and M. Wiescher, Phys. Rev. C **53**, 475 (1996).
[20] C. Iliadis, J. D'Auria, S. Starrfield, W. Thompson, and M. Wiescher, Astrophys. J. Suppl. **134**, 151 (2001).
[21] C. Wrede, Phys. Rev. C **79**, 035803 (2009).
[22] D. W. Bardayan *et al.*, Phys. Rev. C **65**, 032801 (2002).
[23] A. Parikh, J. A. Caggiano, C. Deibel, J. P. Greene, R. Lewis, P. D. Parker, and C. Wrede, Phys. Rev. C **71**, 055804 (2005).
[24] D. W. Bardayan *et al.*, Phys. Rev. C **74**, 045804 (2006).
[25] J. A. Caggiano, W. Bradfield-Smith, R. Lewis, P. D. Parker, D. W. Visser, J. P Greene, K. E. Rehm, D. W. Bardayan, and A. E. Champagne, Phys. Rev. C **65**, 055801 (2002).
[26] Y. Parpottas, S. M. Grimes, S. Al Quraishi, C. R. Brune, T. N. Massey, J. E. Oldendick, A. Salas, and R. T. Wheeler, Phys. Rev. C **70**, 065805 (2004); For corrected reaction rates, see **73**, 049907(E) (2006).
[27] D. Seweryniak *et al.*, Phys. Rev. C **75**, 062801 (2007).
[28] P. N. Peplowski *et al.*, Phys. Rev. C **79**, 032801 (2009).
[29] A. Matic *et al.*, Phys. Rev. C **80**, 055804 (2009).
[30] T. Wakasa *et al.*, Nucl. Instrum. Methods Phys. Res. A **482**, 79 (2002).
[31] M. Fujiwara *et al.*, Nucl. Instrum. Methods Phys. Res. A **422**, 484 (1999).
[32] J. P. Greene and G. P. A. Berg, Nucl. Instrum. Methods Phys. Res. B **241**, 1006 (2005).
[33] A. Matic, Ph.D. thesis, University Groningen, 2007 [http://dissertations.ub.rug.nl/faculties/science/2007/a.matic].
[34] R. A. I. Bell, J. L'Ecuyer, R. D. Gill, B. C. Robertson, I. S. Towner, and H. J. Rose, Nucl. Phys. A **133**, 337 (1969).
[35] W. Bohne, K. D. Buchs, H. Fuchs, K. Grabisch, D. Hilscher, U. Jahnke, H. Kluge, T. G. Masterson, H. Morgenstern, and B. H. Wildenthal, Nucl. Phys. A **378**, 525 (1982).
[36] R. A. Paddock, Phys. Rev. C **5**, 485 (1972).
[37] P. M. Endt, Nucl. Phys. A **521**, 1 (1990).
[38] P. M. Endt, J. Blachot, R. B. Firestone, and J. Zipkin, Nucl. Phys. A **633**, 1 (1998).
[39] P. D. Kunz, DWUCK4, a DWBA reaction code (University of Colorado, Boulder, Colorado, 1987), unpublished.
[40] J.-C. Thomas *et al.*, Eur. Phys. J. A **21**, 419 (2004).
[41] W. A. Fowler, G. R. Caughlan, and B. Zimmermann, Annu. Rev. Astron. Astrophys. **13**, 69 (1975).
[42] W. A. Richter and B. A. Brown, Phys. Rev. C **80**, 034301 (2009).
[43] R. Crowter, *Master's thesis*, University of Surrey, Guildford Surrey, United Kingdom, 2007, unpublished.
[44] NON-SMOKER [http://nucastro.org/nonsmoker.html].
[45] TALYS [http://www-astro.ulb.ac.be/Nucdata/Talys/pcapAL].